




Properties of electrochemically deposited NiTe films prepared at varying dopant concentrations of molybdenum

Imosobomeh L. Ikhioya^{1,2} and Agnes C. Nkele^{1,3,*} 

¹Department of Physics and Astronomy, University of Nigeria, Nsukka 410001, Nigeria

²Department of Physics and Industrial Physics, Nnamdi Azikiwe University, Awka, Anambra State, Nigeria

³Department of Physics, Colorado State University, Fort Collins, USA

Received: 11 January 2023

Accepted: 19 July 2023

Published online:
29 July 2023

© The Author(s), under exclusive licence to Springer Science+Business Media, LLC, part of Springer Nature 2023

ABSTRACT

This novel research centered on synthesizing NiTe film through electrochemical deposition technique. The film was doped with molybdenum at varying molar concentrations of 0.1, 0.2, and 0.3 M. The structure, morphology, elemental, optical, and electrical characteristics of the prepared samples with preferential orientation in the (1 0 0) plane have been investigated. Hexagonal crystal structure with prominent peaks was gotten from the X-ray diffractograms. The surface morphologies showed dense micrograins with high optical absorption while the basic elemental compositions of the deposited films were confirmed from the EDX plots. Optical plots gave maximum absorbance values at the ultraviolet region and reduced reflectance values at increasing molar concentrations. The band gap energy values ranging from 2.01 to 1.68 eV decreased at increasing molar concentrations. The electrical results gave improved electrical conductivity as the dopant concentration increased. The prepared samples find useful application in optical and solar cell devices.

1 Introduction

The demand for clean energy is continuously on the increase. Transition metal chalcogenides have flexible structures, electrochemically stable nature, energy storage abilities, and increased conductivity [1–3]. Their nanostructures have nonlinear optical characteristics that make them relevant in optical storage, catalytic devices, nonlinear refraction, optical sensors, etc. [1, 4]. Transition metal chalcogenides have

flexible characteristics and increased carrier mobility that makes them useful for application in optoelectronic and solar cell devices [5–7]. They also serve as useful tools in hydrogen evolution reactions and charge storage mechanisms [8, 9]. Metal tellurides have unique physical buildup and surface chemistry that encourage their diverse applications [10]. They serve as good energy storage and sensing devices [11]. Tellurium exhibits improved electrical conductivity, high electrochemical activity, and good energy

Address correspondence to E-mail: chinecherem.nkele@unn.edu.ng

storage ability [2]. NiTe is a three-dimensional metal chalcogenide that exhibits different stoichiometry, various crystal phases, and unique chemical features [12]. The metallic property allows NiTe to be used as a highly conductive material [13] and cathode material in hydrogen evolution reactions [8]. NiTe has excellent transport and electrical characteristics that enhances its diverse application areas [2]. The unique crystal structure of NiTe makes it useful for improved catalysis, stability, and electrocatalysis [13]. Several methods of synthesizing NiTe like solvothermal, electrochemical deposition, physical vapor transport, atomic layer deposition, mechanochemical, hydrothermal, chemical vapor deposition, have been reported [8, 11, 12, 14–16]. The properties and performance of NiTe can be improved by doping, annealing, and through the formation of heterogeneous structures [17]. NiTe finds useful application in electrocatalytic systems, energy storage devices, sensors, etc. [18].

Molybdenum has increased free electrons that it can contribute to enhance the electrical and optical properties of the host material [19]. The small ionic radius allows for substitution into the lattice matrix of the host material [20]. Doping involves the addition of impurity to a host material. It ensures better performance, increased conductivity, and efficiency of a device or host material [21]. The carrier concentration of the element is a major factor in making the choice of the dopant. Electrochemical deposition (ECD) involves coating a substrate surface through electrochemical reactions with the as-deposited film acting as the working electrode [22]. It is an affordable, quick, and easy way of synthesizing films while regulating the thickness [23].

De Silva et al. electrodeposited NiTe on glassy carbon electrode for effective catalysis and water splitting [18]. The films also exhibited stable activity and improved catalytic performance owing to their band alignment and electronic structure. The crystal phase of NiTe was tuned by Xiang et al. through a hydrothermal technique [8]. This modification was possible through annealing effects which shifted the d-band lattice center, increased electrochemical activity, and enhanced the performance of hydrogen evolution reaction as an electrocatalyst. NiTe films have been fabricated by transforming Te films electrodeposited in nickel foils [24]. The fabricated material recorded reduced contact resistance with potential use in solar cells. Laminated microsheets of

Ni₃Te₂ have been fabricated as counter electrodes for use in dye sensitized solar cells [11]. The chemical vapor deposited electrodes exhibited hexagonal crystal structure, fibrous morphology, stable cycles over time, and average power conversion efficiency of 10.47%. Nanorods of nickel cobalt telluride were prepared by hydrothermal method to yield highly sensitive films with improved electrochemical performance [4]. It can also serve as an effective energy storage material with improved power density and stable cyclic performance [1]. Microwave-assisted method was useful in producing NiTe electrodes with high specific capacitance of 808.9 F/g and 91% charge retention [13].

This work focused on preparing NiTe films by electrochemical deposition method at varying molar concentrations of the dopant (molybdenum) due to the unique properties and vast applications. This is the first report made on molybdenum-doped NiTe films prepared through electrochemical deposition technique at varying molybdenum concentrations. The characteristics of the prepared films were studied alongside the effects of the dopant (molybdenum) on the NiTe films.

2 Experimental details

2.1 Materials

Analytical grade chemicals like Nickel chloride hexahydrate (NiCl₂·6H₂O), Molybdenum dioxide (MoO₂), telluride dioxide (TeO₂), Hydrogen Chloride (HCl), Ammonia solution (NH₃) were used. Potentiostat supplied DC voltage in a three-electrode cell setup. The electrochemical setup was comprised of a source of cation (i.e., MoO₂, NiCl₂·6H₂O for Mo²⁺, Ni²⁺), anionic source (i.e., telluride dioxide for Te²⁻), deionized water, conducting substrate (Fluorine-doped tin oxide) served as cathode while carbon was used as the anode. The substrates were purified and preserved in air-tight storage.

2.2 Experimental

Electrochemical deposition (ECD) method was utilized in depositing the films. 0.1 M of Telluride dioxide (TeO₂) was solvated in 10 ml of aqueous hydrogen chloride while 0.1 M of Nickel chloride hexahydrate (NiCl₂·6H₂O) was dissolved in 100 ml of

deionized water. Ammonia was added to adjust the pH of the solution to a value of 7.0. The electrochemical bath was stirred with a magnetic stirrer and the electrochemical deposition was carried out for 5 s to produce the NiTe film while stirring the solution. The film was then rinsed, dried, and annealed at 60 °C for 30 min. The dopant solution was made by dissolving 0.1, 0.2, 0.3 M of Molybdenum dioxide (MoO_2) in deionized water and mixing with the NiTe precursor solution in the electrochemical bath. The experimental setup is shown in Fig. 1 while the parameters utilized in this experimental process have been outlined in Table 1.

2.3 Characterizations

The structure, morphology, elemental, optical, and electrical characteristics of the molybdenum-doped and undoped NiTe samples have been investigated respectively through the use of Bruker D8 Advance X-ray diffractometer (XRD) with $\text{Cu-K}\alpha$ line ($\lambda = 1.54056\text{\AA}$), JEOL JSM 6360 scanning electron microscope (SEM), Energy dispersive X-ray spectroscopy (EDX), 756 S UV–Vis Spectrophotometer, and a Four point probe (Model T345).

3 Results and discussion

3.1 Structural analysis

Figure 2 gives the structural plots of the prepared samples. The X-ray diffractograms in Fig. 2a show

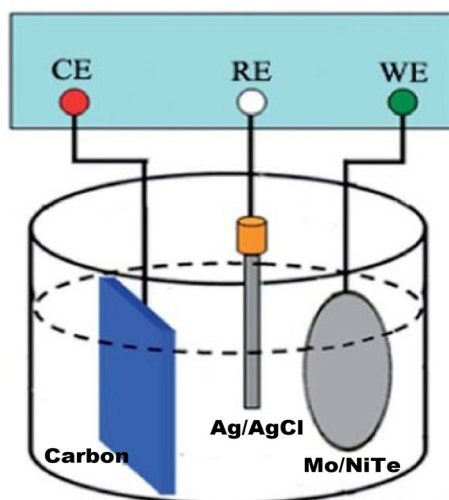


Fig. 1 Schematic illustration of the ECD technique adopted

hexagonal crystal structure with JCPDS card number: 00-038-1393. For this crystal structure, the nickel ions and tellurium ions develop strong synergy that yields the hexagonal lattice structure. The peaks revealed highly crystalline peaks of the films with well-aligned prominent diffraction peaks. The impurity-free patterns confirmed successful formation of the hexagonal crystal structure [13]. Prominent peaks were observed for the synthesized samples with no preferred orientation. The 0.3 M doped sample recorded the most prominent peaks with preferred orientation observed on the (1 0 0) plane. Addition of molybdenum did not significantly distort the crystal structure as there is no observable peak shift due to the small ionic size of the dopant.

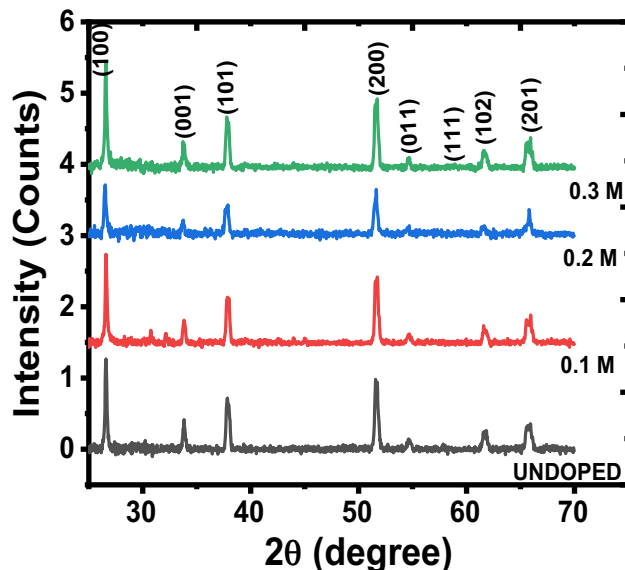
Scherrer's equation [25] ($D = \frac{k\lambda}{\beta \cos \theta}$) was useful in calculating the crystallite size, D (± 5 nm) of the NiTe samples, lattice constants (a , c), interplanar distance (d), and the dislocation densities, δ ($1/D^2$) [26, 27] as shown in Table 2. were obtained from the preferred orientation at (100) plane. The calculated average crystallite size from Table 2. is about 0.81 nm and it gives the relationship between the different structural parameters. The varying crystallite sizes and impurity introduction accounted for the dislocation densities and varying lattice constants. Increase in crystallite size leads to modifications in the lattice sites which accounts for an increase in the 2 theta values and varying lattice constant values. The interplanar distance between the lattice planes have also been shown to vary over the orientation planes [28]. Distortions due to introducing the impurity give room for the dopant to occupy the interstitial position leading to a change in the lattice structure. These distortions account for the peak broadening observed at higher 2 theta values [29]. As the crystallite size got smaller, the peak got broader at larger 2 theta angle values [8].

3.2 Morphological study

Figure 3 gives the surface micrographs of the NiTe samples. The SEM images revealed micrograins spread throughout the substrate surface. Doping the NiTe film at different concentrations gave sticky-like agglomerate due to molybdenum introduction. More prominent agglomerates were observed in the film doped at 0.2 M due to greater particle adhesion in the sample [30]. The morphology also corresponds to the

Table 1 Table showing the deposition parameters varied during the experimental procedure

Sample	NiCl ₂ ·6H ₂ O (ml)	TeO ₂ (ml)	Dopant Conc. (M)	MoO ₂ (ml)	Time (s)	Voltage (V)
NiTe	20	20	0	0	5	10
NiTe/Mo 0.1 M	20	20	0.1	10	5	10
NiTe/Mo 0.2 M	20	20	0.2	10	5	10
NiTe/Mo 0.3 M	20	20	0.3	10	5	10

**Fig. 2** X-ray diffractograms of the doped and undoped NiTe films

random orientation obtained from their structural result [21]. The undoped, 0.1, 0.2, and 0.3 M samples had particle sizes of 6.3, 7.0, 8.2, and 9.1 nm, respectively, as seen in Fig. 3b gotten using ImageJ Software. Average particle size of about 7.65 nm was obtained. Incorporating molybdenum also gave rise to rough surfaces which would facilitate optical and photocatalytic activities [20].

Table 2. Structural parameters of the prepared NiTe films

2θ (°)	hkl	FWHM	D × 10 ⁻² (nm)	a (nm)	c (nm)	d (nm)	δ (nm)
26.42	(100)	0.25	69	0.09	0.16	0.08	2.08
31.10	(001)	0.32	44	0.28	0.49	0.25	5.10
37.91	(101)	0.42	33	0.42	0.74	0.37	8.98
49.41	(200)	0.18	86	0.12	0.20	0.10	1.36
55.10	(011)	0.51	36	0.08	0.15	0.08	7.51
58.30	(111)	0.24	89	0.09	0.16	0.07	1.24
61.40	(102)	0.11	171	0.09	0.15	0.08	0.34
64.62	(201)	0.19	119	0.09	0.16	0.09	0.71

3.3 Elemental studies

The EDX plots of the doped and molybdenum-doped NiTe samples are shown in Fig. 4. Nickel (Ni) and Tellurium (Te) were prominent peaks observed from the spectra while the doped sample revealed the additional presence of molybdenum (Mo) from the dopant. This confirms the presence of the synthesized materials. The elemental compositions of the films in atomic weight (%) have been outlined in Table 3, and increasing atomic percentages of molybdenum confirms the increasing concentrations of the dopant.

3.4 Optical analysis

Figure 5 gives the absorbance and reflectance plots of the undoped and Mo-doped NiTe samples. It can be clearly seen that doping NiTe with molybdenum altered its optical characteristics. Doping with molybdenum increased their absorbance property as maximum absorbance was recorded for the film prepared at 0.3 M. This corresponds to the direct proportionality between absorbance and concentration where more light gets blocked due to the interference of more molecules. Higher concentration of impurities introduced into the host lattice is responsible for the increased absorbance and reduced reflectance at increasing dopant concentrations [31]. These properties make them useful for window

Fig. 3 SEM images of the undoped and Molybdenum-doped NiTe samples

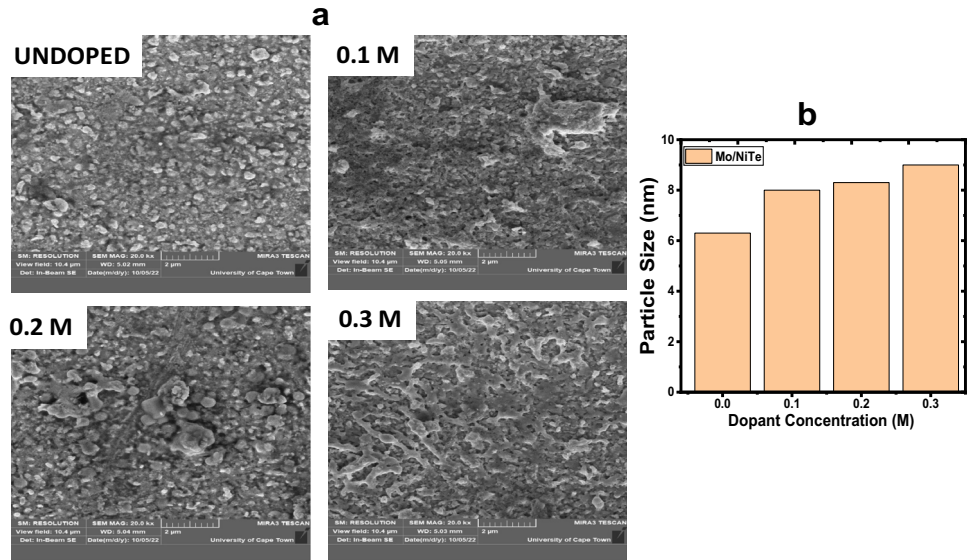


Fig. 4 EDX spectra of the a undoped and b Mo-doped NiTe samples

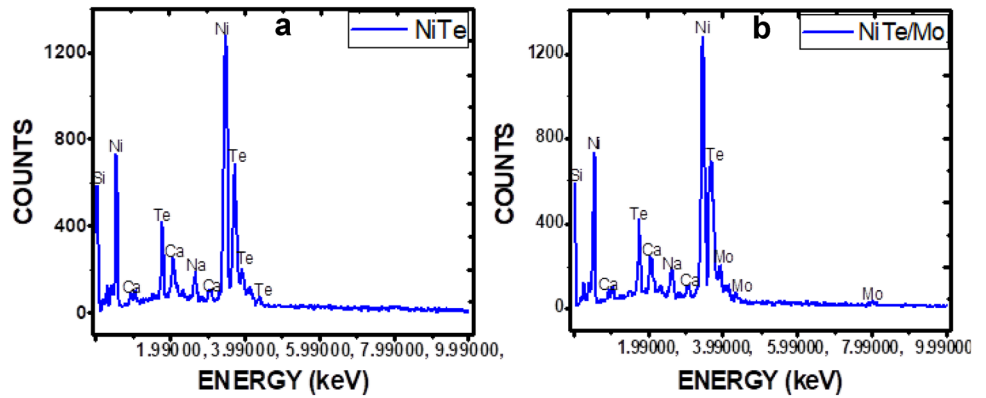


Table 3. Elemental components of the Molybdenum-doped and undoped NiTe samples

NiTe		NiTe/Mo			
Elements	Undoped Atomic weight(%)	Elements	0.1 M Atomic weight (%)	0.2 M Atomic weight (%)	0.3 M Atomic weight (%)
Nickel	56.73	Nickel	53.08	53.08	53.08
Tellurium	36.80	Tellurium	35.80	35.80	35.80
Silicon	5.54	Molybdenum	6.78	6.85	6.96
Calcium	0.80	Silicon	3.41	3.45	3.49
Sodium	0.13	Calcium	0.83	0.82	0.86
		Sodium	0.10	0.10	0.17

coating and optical devices. The refractive index and band gap energy plots of the NiTe films are shown in Fig. 6(a–b). The higher the dopant concentration, the more the refractive index values of the films. This is because the film thickness increases and creates a denser medium which yields higher refractive

indices. This makes the material useful for potential application in optoelectronic devices [24]. Band gap energy plots were estimated from Tauc’s equation and the energies were gotten by extrapolating the linear portion of the graph. The obtained band gap energies are seen in Fig. 5b and give increasing band

Fig. 5 a Absorbance and b reflectance versus wavelength plots of the synthesized NiTe samples

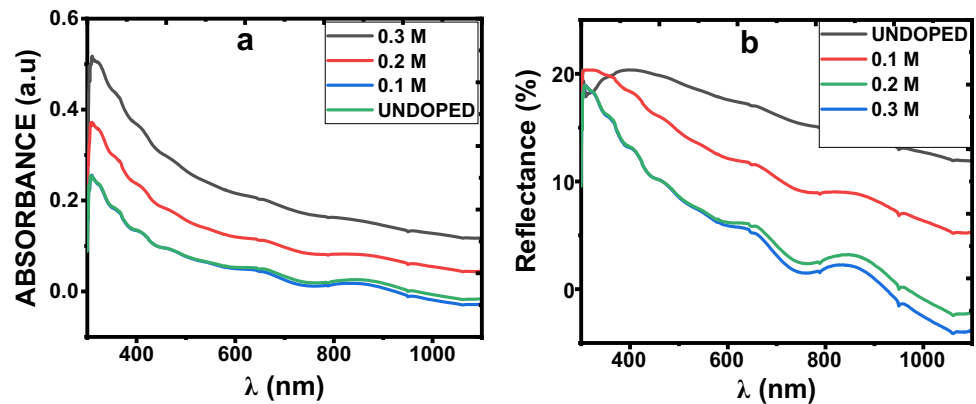
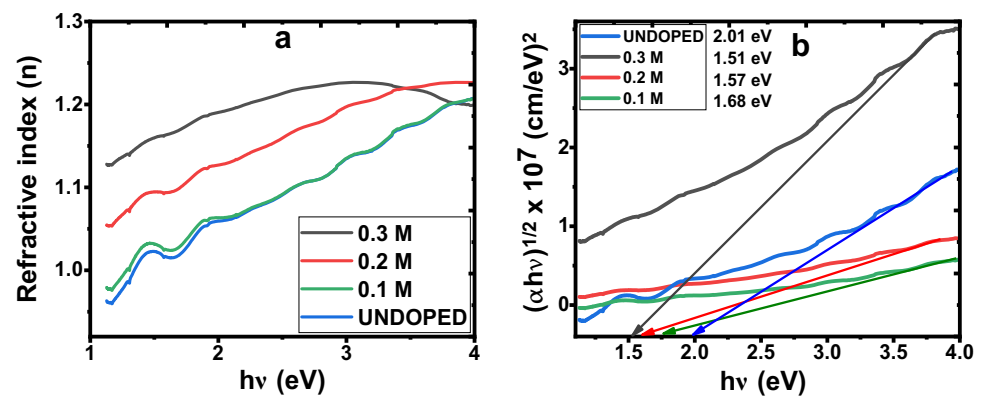


Fig. 6 Plots showing a refractive index versus energy and b energy band gap plots of the synthesized NiTe samples



gap energies as the molar concentrations increased. The reduced band gap energies upon addition of molybdenum could be because the host electrons gained more energy for band transition [12]. The undoped sample recorded higher band gap energy which decreased upon doping with molybdenum. Increasing the concentration of dopant resulted in decreasing band gap energies because increased thickness increases the localized states within the band gap [32]. The low energy band gap makes the films potential photovoltaic materials.

3.5 Electrical studies

Figure 7 gives the electrical plots (resistivity and conductivity versus thickness) of the synthesized samples. It can be observed that increasing the dopant concentration led to an increase in the film thickness and increased conductivity [33, 34]. This trend is due to a reduction in the value of density of surface states at the grain boundaries. The values of the electrical parameters have been outlined in Table 4. Adding molybdenum led to increase in concentration of the synthesized films and

subsequent increase in material conductivity through the addition of extra electrons. The improved electrical properties make the materials potentially useful in solar cells [35].

4 Conclusion

This work successfully synthesized NiTe films prepared through electrochemical deposition. The samples were doped with molybdenum at varying molar concentrations of 0.1, 0.2, and 0.3 M. The structure, morphology, elemental, optical, and electrical characteristics of the NiTe samples were investigated using XRD, SEM, EDX, UV-Vis spectrophotometer, and a Four point probe respectively. Hexagonal crystal structure with prominent peaks was gotten from the XRD results. Micro-grained morphology was observed from the SEM images while the confirmation of constituent elements in the as-deposited film was confirmed. Optical results gave high absorbance values with band gap energy values ranging from 2.01 to 1.68 eV. Increasing the dopant concentration led to more film thickness and

Fig. 7 Plots showing the resistivity and conductivity versus **a** thickness and **b** dopant concentration relationship between the prepared NiTe samples

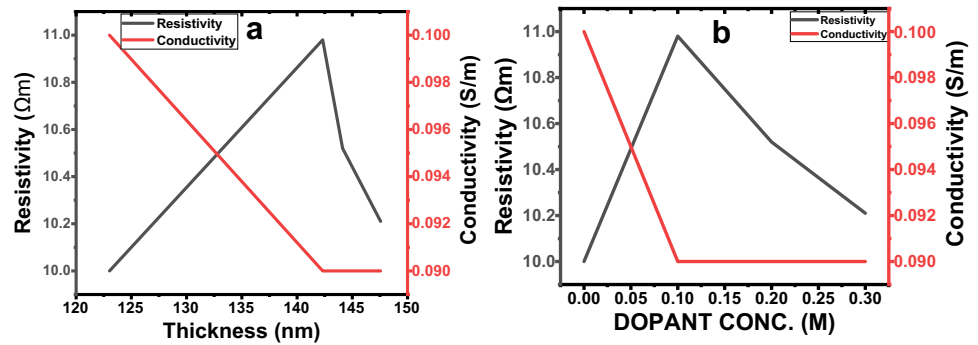


Table 4. Electrical parameters of the undoped and Mo-doped NiTe samples

Samples	Thickness (nm)	Resistivity, $\rho \times 10^{12}$ ($\Omega\text{.cm}$)	Conductivity, $\sigma \times 10^{12}$ (S/m)
NiTe	123.02	10.98	0.091
NiTe/Mo 0.1 M	142.32	10.52	0.095
NiTe/Mo 0.2 M	144.12	10.21	0.098
NiTe/Mo 0.3 M	147.56	10.00	0.100

subsequent electrical conductivity. The prepared samples find potential application in optical, solar cell, and optoelectronic devices.

Author contribution

All authors read and approved the final manuscript. ILI: Conceptualization and experimentation. ACN: Writing manuscript and taking correspondence.

Funding

The authors declare that no funds, grants, or other support were received during the preparation of this manuscript.

Data availability

Data will be made available upon request to the corresponding author.

Declarations

Competing interests The authors have no competing interests to declare that are relevant to this article.

References

1. M. Manikandan, K. Subramani, S. Dhanuskodi, M. Sathish, *Energy Fuels*. **35**, 12527 (2021)
2. N.Y.W. Zaw, S. Jo, J. Park, N. Kitchamsetti, N. Jayababu, D. Kim, *Appl. Clay Sci.* **225**, 106539 (2022)
3. Y.X. Yan, T. Ahmad, X. Zhang, T. Liang, S.U. Rehman, M.U. Manzoor, W. Liu, M.A. Basit, *Mater. Res. Express*. **6**, 076513 (2019)
4. M. Mayilmurugan, G. Rajamanickam, R. Perumalsamy, D. Sivasubramanian, *ACS Omega*. **7**, 14556 (2022)
5. R. Khan, Z.M. Khan, H.B. Aqeel, S. Javed, A. Shafqat, I. Qazi, M.A. Basit, R. Jan, *Sci. Rep.* **10**, 21550 (2020)
6. S. Kimiagar, F. Abrinaei, *Optik*. **272**, 170305 (2023)
7. Z. Dehghani, F. Ostovari, M. Nadafan, *J. Appl. Phys.* **131**, 213101 (2022)
8. Y. Xiang, K. Xiong, L. Yu, H. Zhang, J. Chen, M. Xia, *J. Alloys Compd.* **891**, 161955 (2022)
9. G.M. Lohar, O.C. Pore, R.K. Kamble, A.V. Fulari, in *Nanostructured Materials for Supercapacitors*. ed. by S. Thomas, A.B. Gueye, R.K. Gupta (Springer International Publishing, Cham, 2022), pp.341–357
10. M. L. Aruna Kumari, in *Oxide Free Nanomaterials for Energy Storage and Conversion Applications*, ed. by P. Arunachalam, J. Theerthagiri, A. M. Al-Mayouf, M. Y. Choi, and M. Jagannathan (Elsevier, Amsterdam, 2022), pp. 409–433
11. X.Y. Gu, C.Y. Zhang, J.D. Cheng, S.Q. Kang, K. Wei, G.Z. Sun, X.P. Gao, X.J. Pan, J.Y. Zhou, *Chem. Eng. J.* **442**, 136286 (2022)

12. M. Kristl, S. Gyergyek, S.D. Skapin, J. Kristl, *Nanomaterials* **11**, 1959 (2021)
13. T. Zhang, J. Li, R. Bi, J. Song, L. Du, T. Li, H. Zhang, Q. Guo, J. Luo, *J. Alloys Compd.* **909**, 164786 (2022)
14. H. Ssemwanga, *Electrodeposition of Nickel-Metalloid Alloy Films and Their Investigation for Electrocatalytic Water Splitting*, Thesis, Kyambogo University, 2021
15. S. Pan, M. Hong, L. Zhu, W. Quan, Z. Zhang, Y. Huan, P. Yang, F. Cui, F. Zhou, J. Hu, F. Zheng, Y. Zhang, *ACS Nano*. **16**, 11444 (2022)
16. W.-Y. Jiang, L.-X. Gao, Y. Fan, G. Zhao, F. Chen, S. Cao, Z. Li, J.-Y. Ge, *Phys. Status Solidi (b)*. **259**, 2200037 (2022)
17. C. Dang, S. Yun, Y. Zhang, J. Dang, Y. Wang, Z. Liu, Y. Deng, G. Yang, J. Yang, *Mater. Today Nano*. **20**, 100242 (2022)
18. U. De Silva, J. Masud, N. Zhang, Y. Hong, W.P.R. Liyanage, M. Asle, Zaeem, M. Nath, *J. Mater. Chem. A* **6**, 7608 (2018)
19. U.S. Shenoy, D.K. Bhat, *Energy Adv.* **1**, 9 (2022)
20. A. Jrad, M. Naouai, S. Ammar, N. Turki-Kamoun, *Mater. Sci. Semiconduct. Process.* **130**, 105825 (2021)
21. I.L. Ikhioya, O.B. Uyoyou, A.L. Oghenerivwe, *J. Mater. Sci: Mater. Electron.* **33**, 10379 (2022)
22. I.L. Ikhioya, A.C. Nkele, C.F. Okoro, C. Obasi, G.M. Whyte, M. Maaza, F.I. Ezema, *Optik*. **220**, 165180 (2020)
23. T.R. Kumar, P. Prabukanthan, G. Harichandran, J. Theerthagiri, A.M. Moydeen, G. Durai, P. Kuppusami, T. Tatarchuk, *J. Mater. Sci: Mater. Electron.* **29**, 5638 (2018)
24. Y. Mu, Q. Li, P. Lv, Y. Chen, D. Ding, S. Su, L. Zhou, W. Fu, H. Yang, *RSC Adv.* **4**, 54713 (2014)
25. V. Uvarov, I. Popov, *Mater. Charact.* **58**, 883 (2007)
26. A.C. Nkele, A.C. Nwanya, N.M. Shinde, S. Ezugwu, M. Maaza, J.S. Shaikh, F.I. Ezema, *Int. J. Energy Res.* **44**, 9839 (2020)
27. A.C. Nkele, A.C. Nwanya, N.U. Nwankwo, A.B.C. Ekwealor, R.U. Osuji, R. Bucher, M. Maaza, F.I. Ezema, *Mater. Res. Express.* **6**, 096439 (2019)
28. J. Shen, Q. Zeng, H. Zhang, X. Xi, E. Liu, W. Wang, G. Wu, *J. Magn. Magn. Mater.* **492**, 165661 (2019)
29. A.W. Burton, K. Ong, T. Rea, I.Y. Chan, *Microporous Mesoporous Mater.* **117**, 75 (2009)
30. I. Gosens, J.A. Post, L.J. de la Fonteyne, E.H. Jansen, J.W. Geus, F.R. Cassee, W.H. de Jong, *Part. Fibre Toxicol.* **7**, 37 (2010)
31. C.C. Okorieimoh, U. Chime, A.C. Nkele, A.C. Nwanya, I.G. Madiba, A.K.H. Bashir, S. Botha, P.U. Asogwa, M. Maaza, F.I. Ezema, *Superlattices Microstruct.* **130**, 321 (2019)
32. M. Asaduzzaman, M. Hasan, A.N. Bahar, *SpringerPlus.* **5**, 1–8 (2016)
33. A.C. Nkele, U.K. Chime, A.C. Nwanya, D. Obi, R.U. Osuji, R. Bucher, P.M. Ejikeme, M. Maaza, F.I. Ezema, *Vacuum*. **161**, 306 (2019)
34. I.L. Ikhioya, A.C. Nkele, D.N. Okoli, A.J. Ekpunobi, I. Ahmed, *J. Indian Chem. Soc.* **99**, 100641 (2022)
35. C. Wu, J. Shen, J. Ma, S. Wang, Z. Zhang, X. Yang, *Semicond. Sci. Technol.* **24**, 125012 (2009)

Publisher's Note Springer Nature remains neutral with regard to jurisdictional claims in published maps and institutional affiliations.

Springer Nature or its licensor (e.g. a society or other partner) holds exclusive rights to this article under a publishing agreement with the author(s) or other rightsholder(s); author self-archiving of the accepted manuscript version of this article is solely governed by the terms of such publishing agreement and applicable law.